INTERNATIONAL JOURNAL OF AUTOMOTIVE AND MECHANICAL ENGINEERING
ISSN: 2229-8649 e-ISSN: 2180-1606
VOL. 21, ISSUE 2, 2024, 11386 – 11397
DOI: https://doi.org/10.15282/ijame.21.2.2024.16.0879

RESEARCH ARTICLE

Comparison of Velocity Profiles in Stented Carotid Artery Bifurcation Between Computational Fluid Dynamics and Particle Image Velocimetry Measurements

A. Fahmi Huwaidi M. Noor[1], Nasrul Hadi Johari[1,2]*, Adi Azriff Basri[3], and Xiao Yun Xu[4]

[1]Faculty of Mechanical and Automotive Engineering Technology, Universiti Malaysia Pahang Al-Sultan Abdullah, 26600 Pahang, Malaysia
[2]Centre for Advanced Industrial Technology, Universiti Malaysia Pahang Al-Sultan Abdullah, 26600 Pahang, Malaysia
[3]Department of Aerospace Engineering, Universiti Putra Malaysia, 43400 Serdang, Selangor, Malaysia
[4]Department of Chemical Engineering, Imperial College London, London, United Kingdom

ABSTRACT - Cardiovascular disease remains the leading cause of morbidity and mortality globally, necessitating extensive research into the hemodynamics of blood flow under pathological conditions, such as atherosclerosis in carotid arteries. In vitro studies, particularly Computational Fluid Dynamics (CFD), are crucial for advancing our understanding of arterial blood flow and predicting pathological states. However, the accuracy of CFD simulations relies heavily on their validation against empirical data, such as those obtained from Particle Image Velocimetry (PIV). This study focuses on the comparative analysis of CFD predictions and PIV measurements of blood velocity vectors in a stented carotid artery bifurcation model under steady flow conditions derived from patient-specific data. The methodology involves simulating blood flow within a CFD framework and conducting PIV experiments using a blood-mimicking fluid seeded with particles in a carotid artery bifurcation phantom. The results indicate a reasonable agreement between the axial velocity vector profiles obtained via PIV and those predicted by CFD, with CFD predicting 10% higher than that recorded by PIV, especially in terms of recirculation areas and velocity values, despite some discrepancies in the velocity contours distribution, highlighting potential differences in how each method captures flow separation or recirculation areas. Despite some discrepancies in velocity contour distribution, which highlight potential differences in capturing flow separation or recirculation areas, the findings confirm that CFD simulations can effectively replicate the hemodynamics observed in carotid arteries and potentially other arterial segments. This study emphasizes the importance of integrating CFD simulations with experimental PIV data to validate and refine our understanding of arterial flow dynamics, significantly contributing to cardiovascular research and the development of interventions for arterial diseases.

ARTICLE HISTORY
Received : 18th Feb 2024
Revised : 09th May 2024
Accepted : 29th May 2024
Published : 20th June 2024

KEYWORDS
Carotid artery bifurcation
Stent
Particle Image Velocimetry
Computational Fluid Dynamics
Velocity profiles

1.0 INTRODUCTION

The presence of carotid arterial stenosis impedes cerebral perfusion, significantly elevating the risk of cerebrovascular events such as stroke and transient ischemic attacks [1], [2]. As a prominent contributor to cardiovascular disease (CVD), carotid stenosis often necessitates intervention through invasive medical procedures designed to reestablish and optimize blood flow. Surgical interventions, including carotid endarterectomy, angioplasty, stent deployment, and arterial bypass grafting, are determined by assessing the patient-specific factors, such as age, anatomical pathology, associated surgical risks, and the breadth of clinical expertise [1], [3]. Among these, stent implantation has gained recognition as a minimally invasive alternative for revascularization, thereby reinstating adequate cerebral blood supply [4].

Although Particle Image Velocimetry (PIV) is a relatively recent technique in hemodynamics research, it has quickly become a valuable method for measuring particle velocities within fluids. PIV provides detailed insights into blood flow patterns under both normal and pathological conditions, contributing significantly to our understanding of cardiovascular dynamics. Despite its usefulness, Computational Fluid Dynamics (CFD) offers a more versatile and comprehensive approach to studying blood flow. With higher spatial resolution and the ability to capture a wider range of flow behaviors, CFD is increasingly favored for its detailed analysis capabilities [5]. As a branch of fluid mechanics, CFD employs numerical methods and algorithms to analyze complex fluid flows, making it particularly effective for examining the intricate dynamics of blood flow in stenotic arteries [5].

Particle image velocimetry has become an important tool in hemodynamics research, especially when studying blood flow velocity profiles in arterial models under various pathological conditions [6], [7]. This technique, along with CFD, offers valuable insights into blood flow dynamics. For example, Yujie Li et al. [8] effectively used both PIV and CFD to analyze flow profiles in intracranial aneurysms. Their work demonstrates how these methods can shed light on complex and abnormal flow patterns within cerebral vasculature. Similarly, Ho Geol Woo et al. [9] employed diffusion-weighted imaging to pinpoint atherosclerotic plaque locations. This approach underscores the importance of advanced imaging techniques in the diagnosis and study of atherosclerosis. Furthermore, Patrick et al. [10] conducted PIV experiments to

*CORRESPONDING AUTHOR | Nasrul Hadi Johari | ✉ nhadi@umpsa.edu.my

investigate blood flow in healthy carotid arteries using models that vary in rigidity and compliance. Their research emphasizes the critical need to understand the dynamics of normal arterial flow as a baseline for comparing pathological changes and designing effective treatments. Another study by Medero et al. [11] explored the correlation of flow profiles in the carotid artery between PIV and 4D Magnetic Resonance Imaging (MRI), aiming to validate PIV as a complementary tool for CFD simulations. This study underscores the potential of using PIV to validate CFD models and enhance the accuracy and reliability of computational simulations. DiCarlo et al. [12] examined the effects of varying degrees of stenosis on hemodynamic parameters, discussing the significant alterations in flow profiles associated with increasing stenosis severity. Their findings contribute to a deeper understanding of how stenosis impacts blood flow and the potential for developing targeted treatment strategies.

The primary aim of this article is to present a comprehensive comparison of velocity profiles between CFD predictions and PIV measurements within a patient-specific carotid artery bifurcation model. This paper specifically focuses on various aspects of velocity analysis, including velocity vectors, velocity contours, and the velocity distribution across the full geometry of the artery. An important objective of this study is to assess the accuracy and reliability of CFD simulations in replicating real-world blood flow patterns as observed through PIV, thereby contributing to the advancement of diagnostic and treatment strategies in vascular medicine. This comparison is crucial for validating CFD as a tool for predictive modeling in clinical settings, ultimately enhancing our understanding of hemodynamics in patient-specific arterial structures.

2.0 METHODOLOGY

2.1 Patient Specific Geometry

A 68-year-old male with asymptomatic chronic stenosis—90% narrowed according to NASCET criteria—in the right internal carotid artery underwent evaluation via contrast-enhanced computed tomography angiography (CTA). His medical history led to the recommendation for endovascular treatment with carotid artery stenting. The procedure commenced with the insertion of an 8F guiding catheter via the femoral artery to the affected carotid artery. This was followed by a balloon angioplasty using a 3 mm balloon to predilate the stenotic segment. Subsequently, the balloon was withdrawn, and a self-expanding Wallstent (Carotid WALLSTENT™ 6-8 x 37 mm, Boston Scientific) was deployed across the lesion in the internal carotid artery extending distally to the common carotid artery. A post-stenting dilation was then performed with a 4 mm balloon to optimize stent apposition (Fig. 1). Given the retrospective and anonymized nature of the case review, formal ethical approval was deemed unnecessary [13], [14].

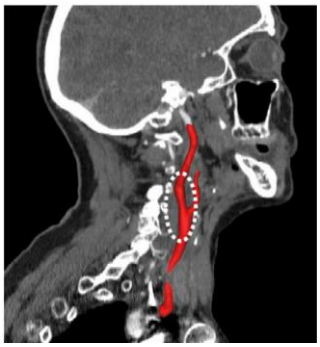

Figure 1. The stented carotid artery obtained a week after the procedure. The image is after a volume rendering and segmentation process of CTA images [13]

The inner contours of the carotid artery were segmented through a combination of thresholding and region-growing algorithms. The process was initiated by identifying the carotid artery bifurcation's lumen as the region of interest (ROI) on transverse plane images. The ROI was delineated by the pixel intensity, a technique applied consistently across all relevant cross-sectional images. Contours of the inner surface were generated from the defined pixels, followed by an application of smoothing algorithms designed to preserve the anatomical accuracy of the vessel's surface. Subsequent to contour generation, a 3D model of the carotid artery bifurcation was constructed by stacking and merging these contours in the coronal plane. This process was carefully monitored to retain critical physiological details throughout the smoothing phase [15]. The post-stent geometry and its central trajectory were outlined using polylines and prepared for transfer to SolidWorks 2020 (Dassault Systems, Velizy, France) for further processing.

To integrate the stent's precise architecture into the fluid domain, especially since post-stent CT scans could not resolve the stent struts due to imaging artifacts [13], a sophisticated virtual implantation technique was applied. The carotid model, encompassing the common carotid artery (CCA), internal carotid artery (ICA), and external carotid artery (ECA), was scaled to twice the size of a standard human artery, with diameters of the CCA at 1.8 cm, and the ICA and ECA at 1.6 cm and 1.4 cm, respectively. Scaled-up geometry is required to enable flow visualization using a high-speed camera during PIV experiments. The same scaled-up geometry was used in all experiments and simulations to avoid flow comparison discrepancies.

The geometry was then translated into a discrete surface mesh and saved as an STL file. The model featured an inlet at the CCA and outlets at the ICA and ECA (as shown in Fig. 2). 3D printing was conducted using stereolithography (SLA) materials, followed by a post-process cleaning with isopropyl alcohol (IPA) to eliminate any residual uncured resin, ensuring the surface reflective index ranged between 1.3 and 1.6 [15].

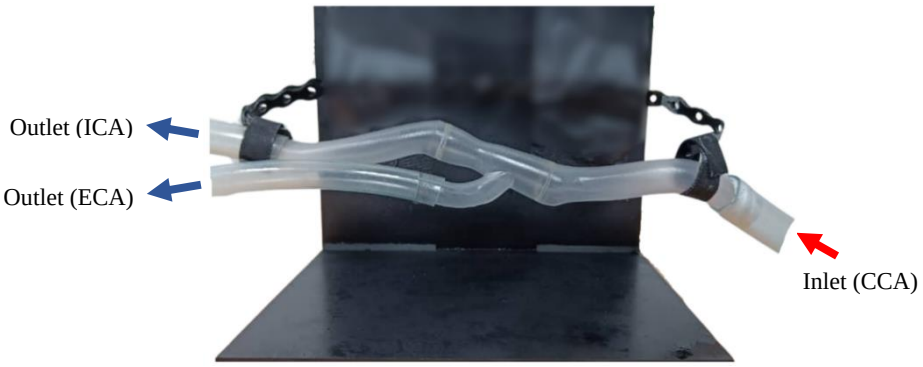

Figure 2. The carotid artery bifurcation phantom

2.2 PIV Experiment

The blood-mimicking fluid (BMF) used in this study is a mixture of water (47.38%), glycerine (36.94%) and sodium iodide NaI (15.68%) using a mixing stirrer. The properties of this solution should replicate the human blood to get real flow features, especially in the human body [6], [12], [16]. The viscosity and density of the BMF mixture are 1244 kg/m^3 and 4.31mPa.s, respectively. The range of refractive index BMF is around 1.40-1.43, which is similar to [17], [18]. Then, the BMF was added with polyamide seeding particles (Dantec Dynamics), 5µm [11]. The seeding particle was used to increase the visibility of flow in the phantom. It was mostly used for flow investigations in liquid and offered suitable tracers to generate sufficient light scattering, high visibility signals, particle density close to water density and excellent traceability to the flow. A safe handling of these particles is guaranteed because of their non-toxic, non-water polluting nature.

In the PIV experiment, the carotid artery phantom was installed to a handler set that connected the inlet CCA and outlets ICA and ECA to the pump via transparent tubes. The pump provides steady flow BMF into the phantom and looping to allow a full cycle. The carotid artery phantom was properly attached to a holder throughout the experiments (Fig. 2). The carotid artery was assembled and connected with transparent tubes at the inlet and outlets. A black cardboard was used to reduce the reflection during the experiment. The equipment setup for the PIV experiment is depicted in Figure 3, showcasing the essential components required to conduct the experiment. These include a geometry phantom, a transparent tube facilitating fluid flow through the phantom, a centrifugal pump, a transverse control connected to the high-speed camera (Flowsense EO 2M) with microlens (AFS-S VR Micro-Nikkor, 105mm f/2.8G, IF-ED), blood mimicking fluid, and a green continuous wave diode laser (Nd: YAG 800 mJ, Dantec Dynamics, Denmark) (135-15Hz). In this experiment, the pump generated a steady flow of 0.82 m/s through the carotid artery geometry phantom. This flow rate is approximately double the average blood velocity in the human carotid artery, which ranges from 0.3 to 0.4 m/s.

The inlet velocity was deliberately doubled to ensure dynamic similarities with the geometry. The calculation of velocity is detailed as follows:

$$Q = A.V \tag{1}$$

$$A = (\pi d^2)/4 \tag{2}$$

$$Re = \frac{\rho V D}{\mu} \tag{3}$$

where Q is the flow rate, A refers to the area, and V refers to the velocity profile. D refers to the diameter of the carotid artery phantom (inlet). Next, Re refers to Reynolds number while μ refers to viscosity. The conservation of mass principle for fluid systems asserts that the mass flow rate into a control volume must equal the mass flow rate out of the control volume. In the PIV experiment, the BMF flow was estimated with a Reynolds number of approximately 4260.

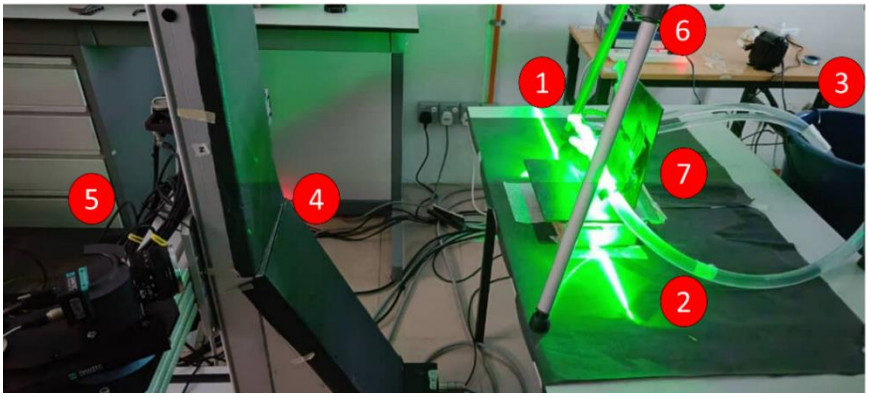

Figure 3. The equipment had been used during PIV. (1) The laser light, (2) connecting tubes, (3) flow pump, (4) transverse platform, (5) high-speed camera, (6) dual laser machine, and (7) the carotid phantom

The calibration method is deemed essential in PIV as it facilitates the acquisition of more accurate and refined results concerning the flow profile through the carotid artery phantom. The transverse control was set to capture the calibration plane perpendicular to the laser (positioned above) and the camera (positioned in front), as illustrated in Figure 3. Subsequently, 100 images were captured in double frame mode using Dynamic Studio software. Key adjustments were made to ensure a clear image and to minimize reflections, which included adjusting the aperture of the high-speed camera, the positioning of the laser through the specimen, and the power of the laser used in the research. Following the image capture phase, the geometry of the carotid artery was masked to isolate specific regions of interest for detailed examination. This masking method was employed to exclude areas not relevant to the investigation.

In the subsequent stages of PIV, image processing techniques were utilized to enhance the clarity and quality of the images. The PIV signal was then applied to ascertain the flow profile of the experiment. The analysis was focused on the velocity profiles in three crucial areas: the inlet, the bifurcation region, and the post-stent area. The research presented in this paper investigated the velocity profiles using velocity vectors, velocity scalar maps, and comprehensive images of flow vectors, providing an in-depth exploration of flow dynamics within these defined areas.

The method to calculate the velocity vectors from the PIV data is cross-correlation. For a pair of images taken at times t and $t + \Delta t$, the cross-correlation R at a displacement (s_x, s_y) in an interrogation window is given by:

$$R(s_x, s_y) = \sum_{x,y} I_1(x, y) \cdot I_2(x + s_{x,}\, y + s_y) \tag{4}$$

where $I_1(x, y)$ is the intensity of the first image at pixel (x, y), $I_2(x, y)$ is the intensity of the second image at pixel (x, y), $s_{x,}$ and s_y are the displacements in the x and y directions, respectively. The peak of the cross-correlation function corresponds to the most probable displacement of particle images between the two frames. This displacement, divided by the time difference Δt between the image pairs, gives the velocity vector (u, v):

$$u = \frac{s_x}{\Delta t}, \qquad v = \frac{s_y}{\Delta t} \tag{5}$$

The algorithms are available in Dynamic Studio (V8, Dantec Dynamics) software, which is directly connected to the PIV measurement system.

2.3 Numerical Simulation

The carotid bifurcation phantom geometry was constructed and subsequently exported into ANSYS FLUENT 19.0 (ANSYS Inc., Canonsburg, PA, USA) for mesh generation and CFD simulations. All geometric dimensions were precisely matched to those of the physical phantom to allow for quantitative comparisons. An unstructured mesh was selected to enhance control over cell distribution, especially in areas near the wall and bifurcation where a denser mesh is crucial due to complex flow dynamics.

Grid independence tests were conducted to align with the specific mesh requirements of the RANS SST-Tran model, comparing velocity profiles generated with meshes of various sizes. The initial mesh, containing 1.1 million elements, was densely populated in the bifurcation area and the mid-region of the stented area, where a transition to turbulence was noted. It was found that peak velocity and wall shear stress (WSS) varied by more than 5% when comparing the 1.1 million-element mesh to a coarser 860,000-element mesh but less than 2% when compared to a finer mesh with 1.5 million elements. As a result, the mesh with 1.1 million tetrahedral elements was chosen for the SST-Tran simulations (Figure 4). Optimal grid resolution near the vessel walls was ensured by maintaining the maximum height of wall cells in wall units (y^+) at approximately 1, with an average value below 0.5.

The study employed the RANS-based SST-Tran model [19], [20], which merges a $k{-}\omega$ model within the boundary layer's inner region with a $k{-}\epsilon$ model in the outer region and free shear flows. This model also incorporates a transitional

model with two additional transport equations, formulated locally for intermittency and the transition onset criterion, based on the momentum thickness Reynolds number. Featuring new correlations for transition, this model has been applied to a wide range of engineering problems, including turbomachinery [19], [21], [22], aircraft configurations, and wind turbines, and has shown promising results in cardiovascular flow applications [13]. The model is available in ANSYS CFX 19.0, and the numerical solution was achieved using an additive correction strategy alongside a coupled algebraic multigrid approach, achieving close to second-order accuracy, following the methodology established by [23].

To simulate physiologically realistic transitional flow, the turbulence intensity level was set at the inlet. Defined as the ratio of the turbulent velocity fluctuations' root mean square to the mean velocity, the turbulence intensity (Tu) was established at 1.5% for the inlet conditions in the SST-Tran simulations. This setting draws on the findings from previous research conducted by [24]. The simulation assumptions included rigid walls with no-slip conditions, ensuring that all velocity components at the wall were zero. The fluid's properties were modeled as Newtonian, matching the kinematic viscosity and density of the fluid utilized in the PIV experiments. In reality, larger vessels like the carotid, aortic segments, and peripheral arteries are commonly treated as Newtonian fluids in simulations [25]–[27].

Blood flow was modeled to be constant, steady, and incompressible, reflecting the Newtonian flow conditions replicated by the experimental steady flow pump. An inlet velocity of approximately 0.82 m/s was applied at the CCA inlet, consistent with the conditions documented in the PIV experiment. This resulted in a fully developed flow profile at the CCA inlet with a Reynolds number of 4260. At the outlets of both the ECA and ICA, a gauge pressure of 0 Pa was maintained. The computational simulations were executed on an Intel® Core™ i5-4500 CPU @ 3.30GHz with 8.00 GB of RAM and a 64-bit operating system, ensuring that the computational framework was robust enough to handle the detailed simulations required for accurate modeling of the flow characteristics within the carotid bifurcation phantom.

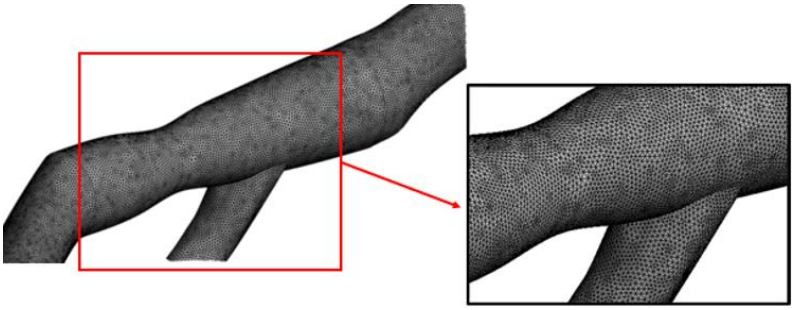

Figure 4. Final mesh of stented carotid bifurcation

4.0 RESULTS AND DISCUSSION

4.1 Region of Interest

Figure 5 illustrates a detailed visualization of the data collection and analysis locales from the PIV experiments and computational simulations conducted on a model of a patient-specific carotid artery. The investigation focused on assessing the flow dynamics at strategic points along the artery under steady flow conditions, utilizing Dynamic Studio software for the analysis of the experimental data.

At Point A, the image delineates the inflow region at the CCA, marking where the blood enters through the inlet with a diameter of 1.8mm. This area is critical for capturing the initial flow conditions and establishing the inlet velocity profile for the simulations. Point B is situated at the bifurcation zone, corresponding to the stented segment where the CCA divides into the ICA. This point is significant due to the complex flow patterns that emerge at bifurcations, which are of particular interest in both clinical assessments and fluid dynamic studies. Point C is demarcated downstream of the stented section, where it is crucial to observe the flow behavior as it evolves after interacting with the stent structure. This region, with a narrower diameter of 1.4mm, is indicative of the flow conditions leading to the peripheral areas of the vasculature.

The precise measurements at each of these points provide a comprehensive profile of the flow patterns, allowing for a detailed comparison between the PIV experimental observations and the numerical simulations. Such comparative analyses are instrumental in validating computational models and in enhancing the understanding of hemodynamics in patient-specific arterial geometries.

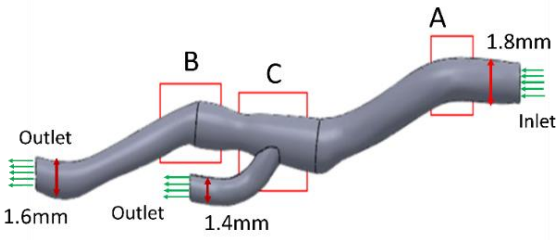

Figure 5. The interest region had been investigated through carotid artery

4.2 Comparison of Velocity Vectors

Table 1 depicts a side-by-side comparison of velocity vectors within a carotid artery geometry, as measured by PIV and predicted by CFD simulation. Observing the PIV results, the velocity vectors appear more diffused, with a wider distribution of velocities and less clarity in the flow direction. This diffusion could be attributed to the experimental limitations of PIV, such as measurement noise, the seeding density of the particles used for tracking the flow, and the optical accessibility of the region.

Conversely, the CFD simulation presents a more coherent and organized pattern of velocity vectors. The flow paths are more distinctly defined, and the vectors follow the geometry's curvature with clear directional flow, which is especially noticeable in the stenotic regions where flow acceleration is expected. This clarity is likely due to the deterministic nature of CFD simulations, which can precisely resolve flow patterns based on the governed Navier-Stokes equations. In terms of similarities, both methods capture the general flow features: the overall direction of flow, areas of flow acceleration, and the presence of complex flow structures such as recirculation zones and vortex formation, which are particularly noticeable in the bifurcation region. The differences, however, are most apparent in the finer details of the flow. The PIV data might show broader regions of mixed velocities due to the physical interplay of particles and the limitations in resolution. The CFD results, given their computational precision, showcase sharper gradients and can predict subtler flow features that might not be as easily captured by PIV, such as very low-velocity zones.

Table 1. The velocity vector between PIV and CFD through full geometry of carotid artery

PIV	CFD
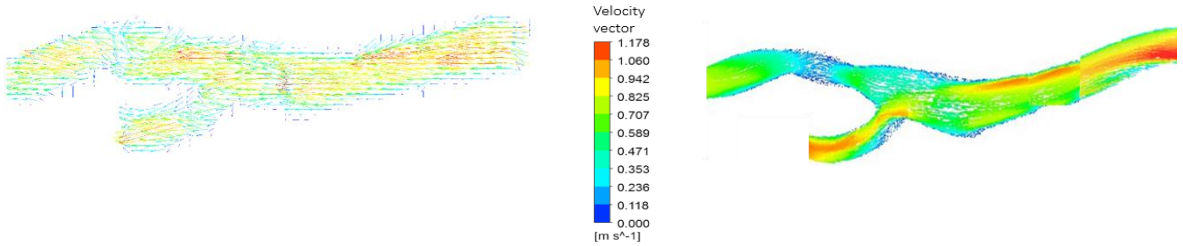	

Table 2 meticulously contrasts the velocity vectors in specific regions of interest (ROI) in the carotid artery as captured through PIV measurements and CFD simulations. The recorded velocity maximum of 1.178 m/s in both results, but with noticeable similarities and differences.

Region A depicts the inflow region at the common carotid artery. The PIV vectors are less coherent, reflecting the inherent variability and measurement noise associated with experimental data. In contrast, the CFD simulation presents a more uniform vector alignment with clearer directionality, as is typical in computational models that do not account for the physiological pulsatility of blood flow. CFD demonstrates higher velocity skewed toward the bottom wall, while PIV portrays higher velocity skewed to both the top and bottom walls. This discrepancy is anticipated, given the non-uniform and slightly chaotic blood flow attributed to the bending and curved shape of the CCA towards the bifurcation.

In region B, the results showcase the flow in the bifurcation area. PIV data reveal more chaotic flow patterns, likely capturing the complex, transitional to turbulent flow behavior that occurs in bifurcations. The CFD simulation suggests smoother flow transition but still captures the presence of disturbed flow, a feature consistent with the fluid dynamics of bifurcations, where flow separation and secondary flows are expected (Perktold and Rappitsch, 1995; Zarins et al., 1983). Both PIV and CFD illustrate a marginal 7% increase in velocity at the entrance of the ECA due to flow splitting in the bifurcation. Pre-bifurcation, low velocities are evident, and upon contact with the artery wall, CFD reveals recirculation flow atop the ICA wall. Johari et al. [13] reported the existence of low-momentum fluid near the wall, giving rise to symmetrical counter-rotating vortices known as Dean vortices in the outer ICA. Intriguingly, these intricate flow patterns elude detection in the PIV measurements. Buchmann and Jermy [28] similarly observed non-uniform velocity profiles in the bifurcation area based on MRI data. Region C focuses on the flow downstream of the bifurcation. The PIV vectors reveal chaotic flow patterns characterized by multiple directional changes, likely induced by the complex bend area. These patterns, possibly helical and secondary flows, are not fully captured by 2D PIV. Conversely, the CFD results in this region display a more structured flow separation pattern. The simulation likely resolves the flow's response to the complex geometry more precisely [29].

Similarities between PIV and CFD are evident in the overall flow direction and the identification of regions where the flow velocity is higher or lower. However, differences arise in the detail and clarity of the flow patterns, with CFD generally providing a more definitive depiction of flow behavior.

Table 2. The velocity vectors comparison at regions of interest between PIV and CFD

Region	PIV	CFD
(a)	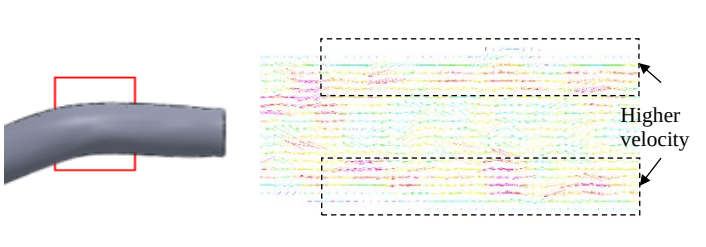	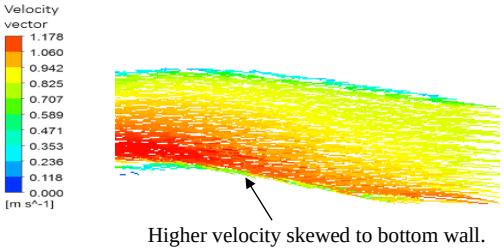
(b)	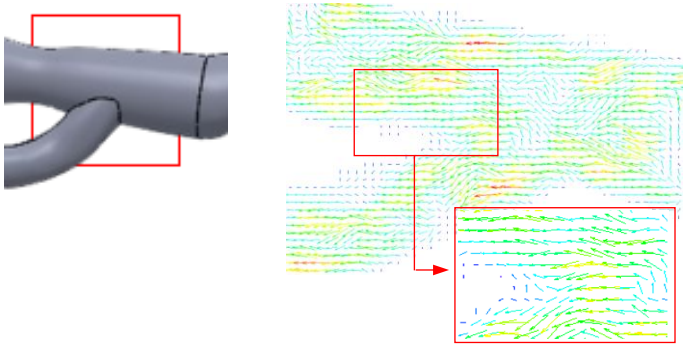	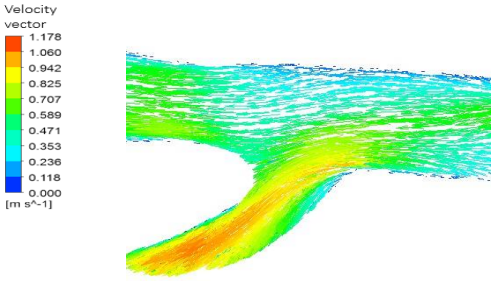
(c)	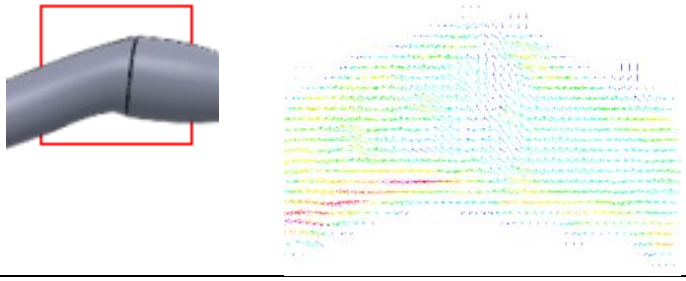	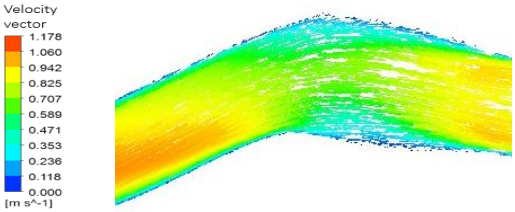

4.3 Velocity Contours

Table 3 illustrates the velocity contours measured in the patient-specific carotid artery. With the interpolated velocity field from the interrogation windows, the contour lines can be drawn to represent regions of constant velocity. The contour algorithms available in Dynamic Studio (V8, Dantec Dynamics) use the marching squares method to trace lines of equal value through the interpolated velocity grid before the refinement and smoothing processes to improve the accuracy and readability of the resulting velocity maps.

In Region A, the PIV contours reveal a broad spectrum of velocities with high heterogeneity, indicative of complex flow patterns likely associated with turbulent or transitional flows within the artery. The CFD contours, while capturing the same general flow pattern, display a smoother gradient of velocity change, typical of the more organized and continuous nature of computational simulation outputs. Region B, located at the bifurcation, shows significant flow complexity in both PIV and CFD results. The PIV contours exhibit pronounced areas of recirculation and flow separation, which are somewhat mirrored in the CFD simulation, though with less pronounced turbulence. This could be due to the CFD model's inherent ability to resolve the flow smoothly, potentially underestimating localized turbulence. In Region C, both PIV and CFD contours suggest a reattachment of flow and the development of a more organized flow pattern. However, the PIV contours suggest greater flow instability and the presence of vortices, while the CFD simulation indicates a relatively orderly re-establishment of organized flow. The curvature, radius, and flow velocity collectively contribute to the generation of secondary vortex pairs in this dynamic system [28].

Table 3. The velocity contours at regions of interest in PIV measurements and CFD

Region	PIV	CFD
(a)	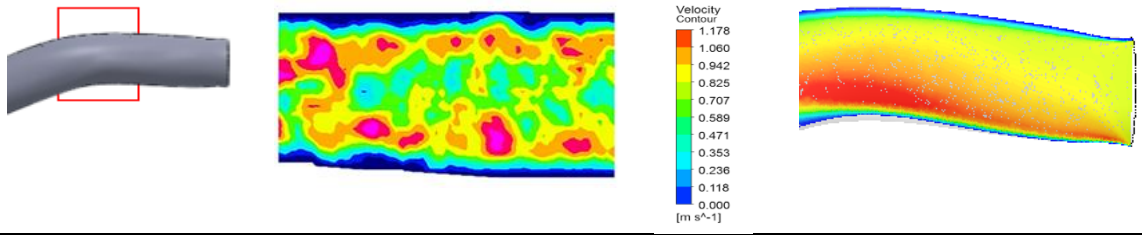	

Table 3. (cont.)

Region	PIV	CFD
(b)	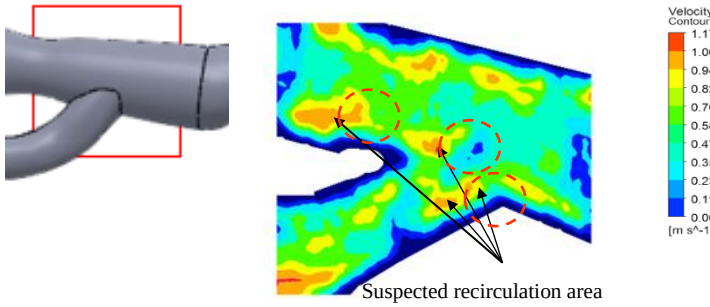	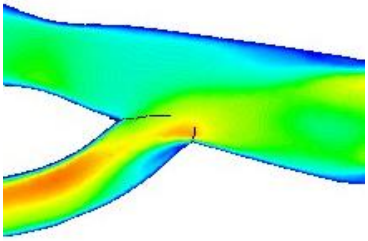
(c)	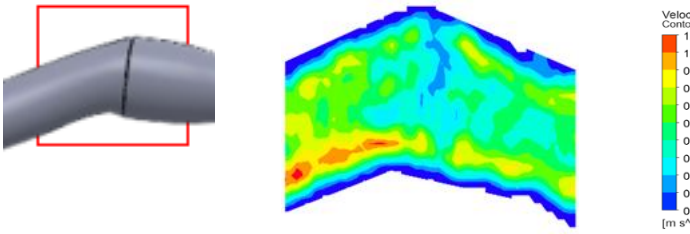	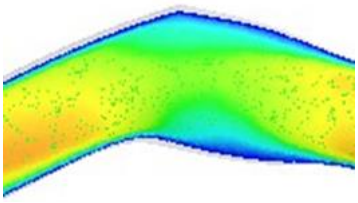

4.4 Axial Velocity Comparison at Different Locations

Table 4 presents axial velocity profiles at two locations (A and B) within three different regions of the carotid artery, displaying a comparison between the PIV measurements and CFD predictions. In the first region, the PIV and CFD profiles at location A exhibit a parabolic shape with an 'm-shaped' axial velocity at the middle of the cross-sectional line, indicating that the flow struggles to achieve full uniformity [26]. Both PIV and CFD also recorded the highest velocity at similar locations, not far from the top wall of the artery. CFD predicts a slightly higher maximum velocity of 0.98 m/s, about 10% higher than recorded in PIV. The profiles show the velocity dropping off towards the vessel walls due to the no-slip condition. At location B, both PIV and CFD indicate a similar trend, but the PIV data show a slightly flattened peak, which could suggest the presence of a more disturbed flow or measurement variability.

In the second region, i.e., the bifurcation area, at location A, the PIV profile indicates a skewed distribution with a peak shifted towards one wall, suggesting the presence of secondary flows or the beginning of a complex flow pattern such as the initiation of a bifurcation or curvature in the vessel. The CFD profile, while also skewed, seems to predict a more pronounced higher velocity close to the bottom wall, possibly due to the model's more precise capture of the flow dynamics and boundary conditions. Nevertheless, both PIV and CFD recorded almost similar peak axial velocity values in the middle of the artery, approximately 0.65 m/s. At location B, both measurements capture a peak velocity, but with disparities in the exact position of the peak, highlighting potential differences in how each method captures flow separation or recirculation areas. This finding supports the [27] study, which concluded that low velocity occurs around the bifurcation in a carotid artery.

The third region's profiles at location A depict a more uniform distribution of velocities across the diameter in both PIV and CFD, suggesting a recovery of laminar flow after a disturbance. However, the PIV profile shows a less pronounced peak, which could be influenced by the experimental setup's spatial resolution limitations. At location B, both PIV and CFD suggest a skewed profile, but CFD shows a sharper velocity gradient, potentially due to its higher sensitivity to localized flow phenomena.

The presence of recirculation flow and low-velocity zones in this region may promote the accumulation of inflammatory compounds, such as low-density lipoprotein (LDL) particles, on the artery wall, potentially leading to the formation of atherosclerotic plaques [30]. Meanwhile, downstream of the stented region, both CFD and PIV results accurately replicate the velocity magnitudes with slight variations, demonstrating the flow pattern's shape near the center and indicating the influence of the flow divider. As reported by [7] in their investigation comparing LES, SST-Trans, and PIV on the stenosed carotid artery bifurcation, a small dent in the axial velocity profile near the center was observed. At all points, the PIV measurements showed slightly lower velocities compared to CFD predictions.

Table 4. Axial velocity profiles comparison at Location A and B

Region	Velocity Profiles	
	(A)	(B)
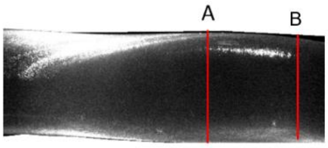	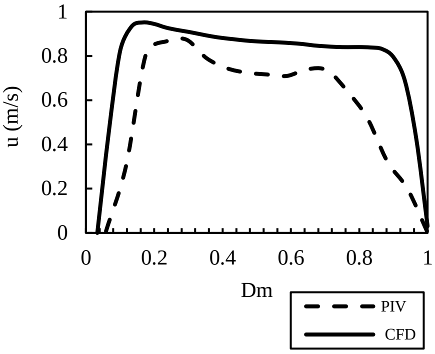	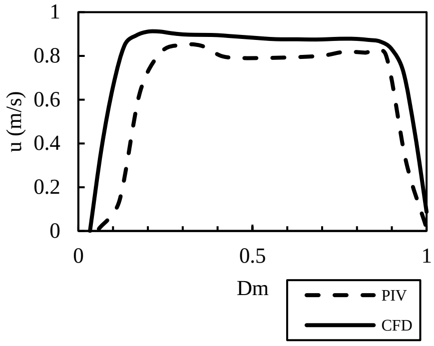
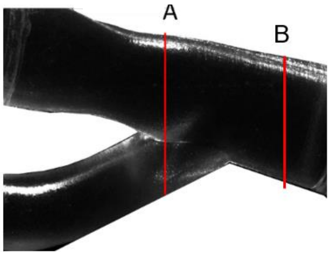	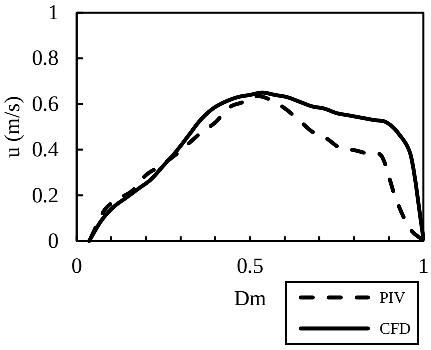	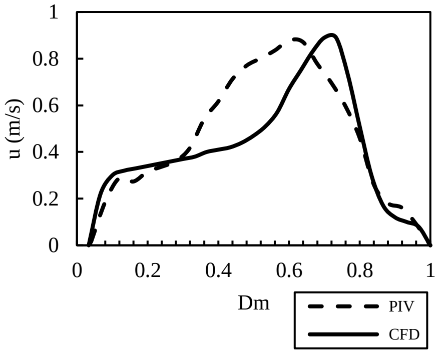
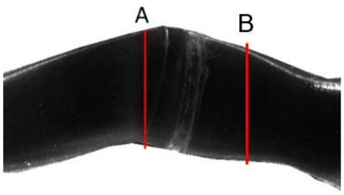	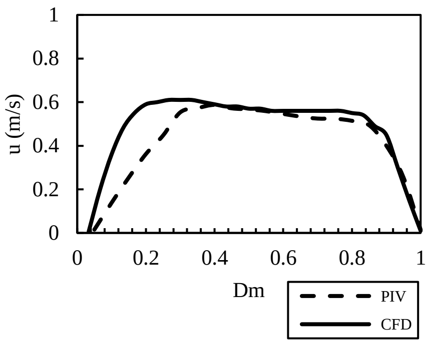	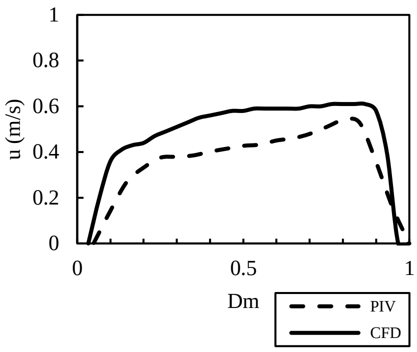

4.5 Discussion

The choice of specific location lines for delineating the internal carotid artery curve area was inspired by previous research, notably the work of studies employing dual lines for comparative velocity profile analysis in the ICA using computational models [31] and others who utilized various cross-sectional lines with PIV to examine flow profiles at the ICA, comparing their findings with MRI data [11].

The ICA's pronounced curvature, compared to the external carotid artery in bifurcation models, leads to flow separation primarily along the outer wall of the ICA, channeling increased flow towards its inner wall. This phenomenon aligns with clinical observations and is a critical factor in understanding bifurcation flow dynamics [32]. Although PIV measurements' color contour maps may not clearly show flow separation in bifurcation areas, the "waist" shape's concentration of higher velocity flow post-bifurcation underscores the radial pressure gradient's role caused by sudden diameter reduction. These observations are in harmony with findings by researchers who investigated the effects of sinus size and position on hemodynamic parameters within the carotid artery, noting particularly low-recirculating velocities near the sinus bulb, which could predispose these areas to atherosclerotic changes [33]. Differences in flow velocities, as observed between PIV and CFD, could indicate potential discrepancies in assessing the severity of stenosis or the effectiveness of stents placed within the arteries. This directly affects treatment planning and outcomes.

The precision of PIV data may be influenced by factors like spatial and temporal resolution camera capabilities, and the accuracy of PIV data can be affected by several factors, including spatial and temporal resolution, camera capabilities, and calibration method precision. Limitations in cross-sectional line placement through patient-specific models may lead to incomplete velocity range capture in the flow field, as evidenced by a study that found less than a 5% average velocity

magnitude difference between PIV and CFD results [34]. Similar studies have evaluated flow patterns in intracranial aneurysms using PIV, CFD, and MRI, underscoring the nuanced interplay between the strengths and limitations of PIV and CFD methodologies [34].

The discrepancies in velocity patterns observed between PIV and CFD approaches underscore the necessity for a detailed and nuanced understanding of flow dynamics within the carotid artery bifurcation. A thorough examination of specific regions within the carotid geometry is crucial for identifying similarities or differences between PIV and CFD outcomes, enhancing our comprehension of complex flow behaviors in this intricate vascular structure. Both PIV and CFD can identify flow separation and recirculation zones, which are critical in understanding the formation and progression of atherosclerotic plaques. However, discrepancies in how these areas are characterized by each method can lead to different interpretations of risk areas for plaque formation.

Overall, both PIV and CFD methodologies offer valuable insights into the flow patterns within the carotid artery geometry. Their comparative analysis not only demonstrates CFD's potential for detailed flow analysis but also emphasizes the significance of PIV in validating and refining computational models. Also, the ability to accurately discern and interpret the differences in flow conditions as reported by PIV and CFD can significantly influence the understanding of disease mechanisms in the carotid arteries and, by extension, patient management strategies.

Future studies should aim to reduce these discrepancies through advanced computational techniques and better experimental setups, enhancing both the reliability of these methods and their applicability in clinical settings. Then, findings from both approaches can be integrated to provide a more precise, accurate, and comprehensive understanding of carotid artery flow dynamics.

5.0 CONCLUSIONS

This study aimed to compare and validate CFD simulations with PIV results within patient-specific models of the carotid artery under healthy conditions. The analysis encompassed various regions of interest, including velocity vectors, scalar maps of velocity, and cross-sectional lines. Notably, velocity vectors in the post-stent area exhibited similar flow behavior between PIV and CFD. However, differences were observed, particularly in the inlet region of the common carotid artery, where PIV indicated lower velocities compared to those predicted by CFD. Specifically, CFD predicted a slightly higher maximum velocity of 0.98 m/s, approximately 10% higher than recorded by PIV. These differences can be attributed to the limitations and deficiencies inherent in the experimental setup, including the boundary conditions of the blood-mimicking fluid, among other factors.

The study highlights the importance of both PIV and CFD methodologies in understanding the hemodynamics within complex vascular geometries under physiological conditions. It emphasizes the need for rigorous calibration of experimental setups and refinement of computational models to closely align the simulations with empirical observations. The findings underscore the potential for an integrated approach, combining experimental and computational techniques, to advance the understanding of cardiovascular dynamics. This approach is crucial for improving therapeutic interventions and the design of vascular prostheses. Addressing the discrepancies identified between PIV and CFD through advanced modeling techniques and improved experimental setups is essential for enabling more accurate and predictive analyses of cardiovascular flows.

6.0 ACKNOWLEDGEMENT

The authors would like to thank the Ministry of Higher Education for providing financial support under the Fundamental Research Grant Scheme (FRGS) No. FRGS/1/2021/TK0/UMP/02/8 (University reference RDU210109).

7.0 REFERENCES

[1] T. Nezu and N. Hosomi, "Usefulness of carotid ultrasonography for risk stratification of cerebral and cardiovascular disease," *Journal of Atherosclerosis and Thrombosis*, vol. 27, pp. 1023–1035, 2020.

[2] F. Mach, C. Baigent, A.L. Catapano, K.C. Koskinas, M. Casula, L. Badimon et al., "2019 ESC/EAS Guidelines for the management of dyslipidaemias: Lipid modification to reduce cardiovascular risk," *European Heart Journal*, vol. 41, no. 1, pp. 111–188, 2020.

[3] V. Aboyans, J.-B. Ricco, M.-L. E L Bartelink, M. Björck, M. Brodmann, T. Cohnert et al., "2017 ESC guidelines on the diagnosis and treatment of peripheral arterial diseases, in collaboration with the European Society for Vascular Surgery (ESVS) Document covering atherosclerotic disease of extracranial carotid Endorsed by : The European Stro," *European Heart Journal*, vol. 39, no. 9, pp. 763–821, 2018.

[4] F.S. Ali, O. Arevalo, S. Zorofchian, A. Patrizz, R. Riascos, N. Tandon, et al., "Cerebral radiation necrosis: Incidence, pathogenesis, diagnostic challenges, and future opportunities," *Current Oncology Reports*, vol. 21, no. 66, pp. 1–17, 2019.

[5] V. Carvalho, I. Maia, A. Souza, J. Ribeiro, P. Costa, H. Puga et al., "In vitro biomodels in stenotic arteries to perform blood analogues flow visualizations and measurements: A review," *Open Biomedical Engineering Journal*, vol. 14, no. 1, pp. 87–102, 2021.

[6] A.F.H.M. Noor and N.H. Johari, "Brief review on recent technology in particle image velocimetry studies on hemodynamics in carotid artery," in *Lecture Notes in Mechanical Engineering*, pp. 267–277, 2022.

[7] N.H. Johari, N. B. Wood, Z. Cheng, R. Torii, M. Oishi, M. Oshima et al., "Disturbed flow in a stenosed carotid artery bifurcation: Comparison of RANS-based transitional model and LES with experimental measurements," *International Journal of Applied Mechanics*, vol. 11, no. 4, pp. 1–21, 2019.

[8] Y. Li, D.I. Verrelli, W. Yang, Y. Qian, and W. Chong, "A pilot validation of CFD model results against PIV observations of haemodynamics in intracranial aneurysms treated with flow-diverting stents," *Journal of Biomechanics*, vol. 100, p. 109590, 2020.

[9] H.G. Woo, S.H. Heo, E.J. Kim, D. Il Chang, T.J. Song, and B.J. Kim, "Atherosclerotic plaque locations may be related to different ischemic lesion patterns," *BMC Neurology*, vol. 20, no. 1, pp. 1–7, 2020.

[10] P.H. Geoghegan, M. . Jermy, and D.S. Nobes, "A PIV comparison of the flow field and wall shear stress in rigid and compliant models of healthy carotid arteries," *Journal of Mechanics in Medicine and Biology*, vol. 17, no. 3, pp. 1–16, 2017.

[11] R. Medero, C. Hoffman, and A. Roldán-Alzate, "Comparison of 4D flow MRI and particle image velocimetry using an in vitro carotid bifurcation model," *Annals of Biomedical Engineering*, vol. 46, no. 12, pp. 2112–2122, 2018.

[12] A.L. DiCarlo, D.W. Holdsworth, and T.L. Poepping, "Study of the effect of stenosis severity and non-Newtonian viscosity on multidirectional wall shear stress and flow disturbances in the carotid artery using particle image velocimetry," *Medical Engineering & Physics*, vol. 65, pp. 8–23, 2019.

[13] N.H. Johari, M. Hamady, and X.Y. Xu, "A Computational Study of the Effect of Stent Design on Local Hemodynamic Factors at the Carotid Artery Bifurcation," *Artery Research*, vol. 26, no. 3, pp. 161–169, 2020.

[14] N.H. Johari, M. Hamady, and X.Y. Xu, "Fluid-structure interaction study of the effect of stent on local hemodynamics parameters at the stented carotid artery bifurcation," *Journal of Advanced Research in Applied Sciences and Engineering Technology*, vol. 28, no. 2, pp. 247–255, 2022.

[15] N.H. Johari, K. Osman, Z.M. Salleh, J. Haron, and M.R.A. Kadir, "The effect of different locations of tracheal stenosis to the flow characteristics using reconstructed CT-scanned image," *Journal of Mechanics in Medicine and Biology*, vol. 12, no. 4, pp. 1–15, 2012.

[16] S. Muda, S. Hwei, Y. Ng, A.S. Shuib, and S.W. Phang, "Development of blood mimicking fluid suspension using polymer particles development of blood mimicking fluid suspension using polymer particles," in *AIP Conference Proceedings*, 2019, vol. 2137, p. 020012.

[17] A. Shuib, P. Hoskins, and W. Easson, "Experimental investigation of particle distribution in a flow through a stenosed artery," *Journal of Mechanical Science and Technology*, vol. 25, no. 2, pp. 357–364, 2011.

[18] P.H. Geoghegan, N.A. Buchmann, C.J.T. Spence, S. Moore, and M. Jermy, "Fabrication of rigid and flexible refractive-index-matched flow phantoms for flow visualisation and optical flow measurements," *Experiments in Fluids*, vol. 52, pp. 1331–1347, 2012.

[19] R.B. Langtry and F.R. Menter, "Correlation-based transition modeling for unstructured parallelized computational fluid dynamics codes," *AIAA Journal*, vol. 47, no. 12, pp. 2894–2906, 2009.

[20] F.R. Menter, "Two-equation eddy-viscosity turbulence models for engineering applications," *AIAA Journal*, vol. 32, no. 8, pp. 1598–1605, 1994.

[21] M.A. Abdul Halim, N.A.R. Nik Mohd, M.N. Mohd Nasir, and M.N. Dahalan, "The evaluation of k-ε and k-ω turbulence models in modelling flows and performance of S-shaped diffuser," *International Journal of Automotive and Mechanical Engineering*, vol. 15, no. 2, pp. 5161–5177, 2018.

[22] I. Saad and S. Bari, "CFD investigation of in-cylinder air flow to optimize number of guide vanes to improve CI engine performance using higher viscous fuel," *International Journal of Automotive and Mechanical Engineering*, vol. 8, pp. 1096–1107, 2013.

[23] B.R. Hutchinson and G.D. Raithby, "A multigrid method based on the additive correction strategy," *Numerical Heat Transfer*, vol. 9, no. 5, pp. 511–537, 1986.

[24] F.P.P. Tan, G. Soloperto, S. Bashford, N.B. Wood, S. Thom, A. Hughes, and X.Y. Xu, "Analysis of flow disturbance in a stenosed carotid artery bifurcation using two-equation transitional and turbulence models," *Journal of Biomechanical Engineering*, vol. 130, no. 6, pp. 1–12, 2008.

[25] D. Wang, F. Serracino-Inglott, and J. Feng, "Numerical simulations of patient-specific models with multiple plaques in human peripheral artery: a fluid-structure interaction analysis," *Biomechanics and Modeling in Mechanobiology*, vol. 20, no. 1, pp. 255–265, Feb. 2021.

[26] D. Quemada, "Rheology of concentrated disperse systems II. A model for non-newtonian shear viscosity in steady flows," *Rheologica Acta*, vol. 17, no. 6, pp. 632–642, 1978.

[27] H. Liu, L. Lan, J. Abrigo, H.L. Ip, Y. Soo, D. Zheng et al., "Comparison of newtonian and non-newtonian fluid models in blood flow simulation in patients with intracranial arterial stenosis," *Frontiers in Physiology*, vol. 12, pp. 1–11, 2021.

[28] N.A. Buchmann, C.V. Nguyen and M.C. Jermy, "Experimental investigation of carotid artery haemodynamics in an anatomically realistic model," vol. 1, no. 2, pp. 172–192, 2009.

[29] H. Zhou, L. Meng, W. Zhou, L. Xin, X. Xia, S. Li et al., "Computational and experimental assessment of influences of hemodynamic shear stress on carotid plaque," *BioMedical Engineering OnLine*, vol. 16, no. 1, pp. 1–11, 2017.

[30] N.H. Johari and M. Hamady, "Computational modeling of low-density lipoprotein accumulation at the carotid artery bifurcation after stenting," *International Journal for Numerical Methods in Biomedical Engineering*, vol. 39, no. 12, p. e3772, 2023.

[31] S. Z. Zhao *et al.*, "Blood flow and vessel mechanics in a physiologically realistic model of a human carotid arterial bifurcation," *Journal of Biomechanics*, vol. 33, no. 8, pp. 975–984, 2000.

[32] A.H. Ningappa, S. Patil, G.S. Belur, A.B.V. Barboza, N. Kumar, R.P. Ballambat et al., "Influence of Altered Pressures on Flow Dynamics in Carotid Bifurcation System Using Numerical Methods," *J. Adv. Res. Fluid Mech. Therm. Sci.*, vol. 97, no. 1, pp. 47–61, 2022.

[33] M. Nagargoje and R. Gupta, "Effect of sinus size and position on hemodynamics during pulsatile flow in a carotid artery bifurcation," *Computer Methods and Programs in Biomedicine*, vol. 192, p. 105440, 2020.

[34] C. Roloff, D. Stucht, O. Beuing, and P. Berg, "Comparison of intracranial aneurysm flow quantification techniques: Standard PIV vs stereoscopic PIV vs tomographic PIV vs phase- contrast MRI vs CFD," pp. 1–8, 2018.